CERN-ACC-NOTE-2018-0028
26-03-2018
marcel.rosenthal@cern.ch

Magnetic Field Measurements of the GOLIATH Magnet in EHN1

M. Rosenthal[1], *N. Charitonidis*[1], *P. Chatzidaki*[1,2], *R. Margraf*[1,3], *H. Wilkens*[1], *F. Bergsma*[1], *P.-A. Giudici*[1]

[1] CERN, 1211 Geneva 23, Switzerland
[2] National Technical University of Athens, School of Appl. Mathematics and Physics, Athens, Greece
[3] Lehigh University, Bethlehem, Pennsylvania, USA

Abstract

This note describes the measurement campaign of the magnetic field of the GOLIATH magnet conducted in 2017. It documents the applied measurement procedure and the consecutive analysis of the recorded data. The shape of the magnetic field along the beam axis is discussed and compared with a previous measurement taken in the 1980s. Overall a very good agreement of both data sets is observed. The integrated vertical magnetic field is obtained by analytical descriptions fitted to the data. Additionally, the influence of different configurations of the power converters, as for example in the case of a different powering scheme of the upper and lower coil of the GOLIATH magnet, on the magnetic field are discussed.

Keywords: GOLIATH, EHN1, H4, Spectrometer magnet, Magnetic field map

Contents

1 Introduction

The GOLIATH magnet is a large spectrometer dipole magnet located in the H4 beamline in the North Area facility of CERN [1] (see Figure 1). It has external dimensions of $4.5\,\mathrm{m} \cdot 3.6\,\mathrm{m} \cdot 2.79\,\mathrm{m}$ [2] and is powered by two power converter sets designated "GOLIATH" and "DAVID" as shown in Figure 2. The magnetic field is generated by two coils wound around the top and bottom yoke, respectively. Each one of the coils has a different number of windings. The power converter set "GOLIATH" is capable of providing a current up to $3600\,\mathrm{A}$ to both coils. However, due to the different number of windings, the magnetic field produced in the bottom coil is less than in the field in the upper. To compensate for this and provide a homogeneous magnetic field, a second power converter ("DAVID") provides an additional current to the bottom coil. For the maximum current in the "GOLIATH" power converter set of $3600\,\mathrm{A}$ an additional current of $1750\,\mathrm{A}$ is needed in "DAVID" to equalize the fields produced by both coils.

The magnetic field of the GOLIATH magnet had been measured by the NA57 collaboration in the 1980s [4], but to the authors best knowledge, neither details for the measurement procedure nor the

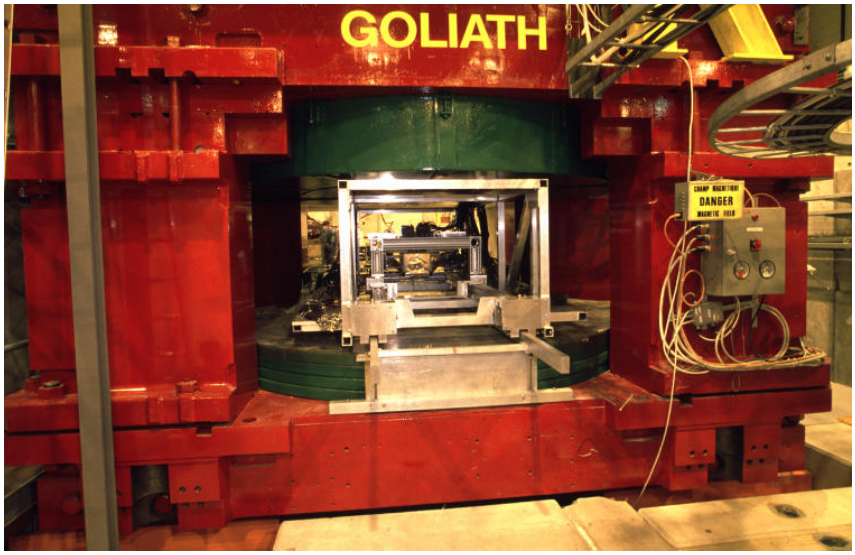

Fig. 1: The GOLIATH Magnet. [1]

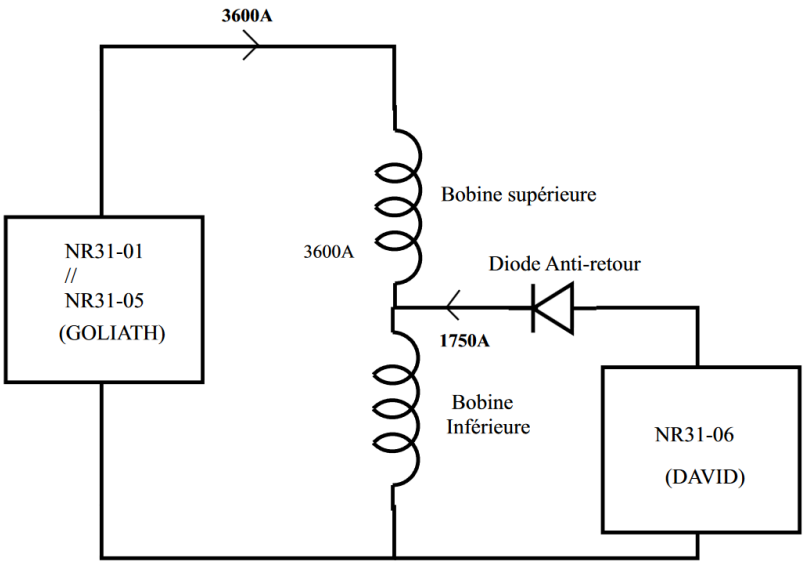

Fig. 2: Sketch of the power converters connected to the two coils of the GOLIATH Magnet. [3]

experimental equipment used at the time were ever published. In addition, different powering schemes of the two power converter sets leading to an asymmetric field configuration have been recently used by various experiments. In order to meet the high demand of precise field information in different power converter configurations, a new measurement campaign using modern equipment and specialized field probes was performed in 2017. The purpose of this campaign was to verify the reproducibility of magnetic field strength and shape, as well as to provide a detailed and consistent documentation of the field map directly usable by the experiments.

2 Measurement Method

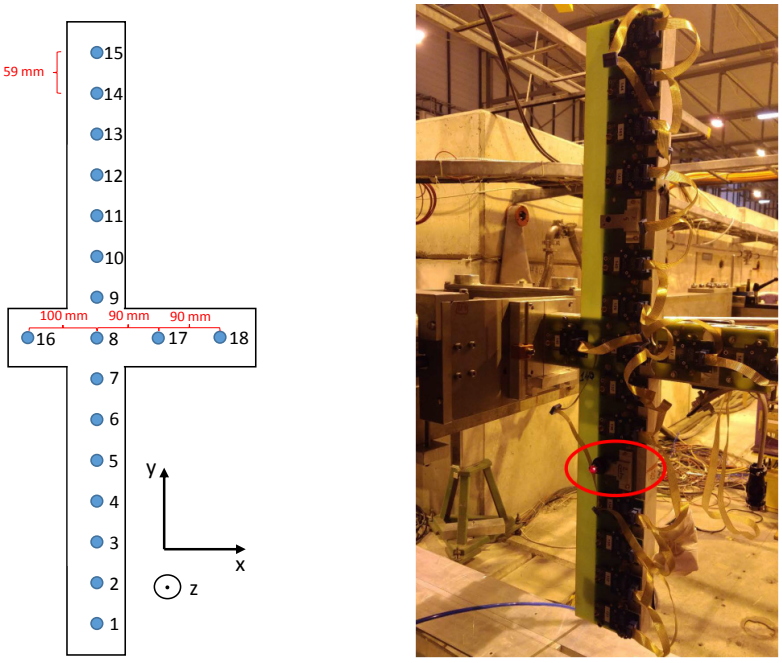

(a) (b)

Fig. 3: Arrangement of the 18 hall probes used during the measurement campaign. [5]

The magnetic field measurements were performed by a set of 18 Hall probes as shown in Figure 3. A subset of 15 Hall probes are separated by $59\,\mathrm{mm}$ in vertical direction. In the following sections this direction will be associated with the y-axis pointing towards the roof of EHN1. The probes 16, 17 and 18 are located in the horizontal direction perpendicular to the beam axis. This axis is associated with the x-axis of the chosen coordinate system pointing towards the left ("Jura"). Probe 16 has an offset of $x = -100\,\mathrm{mm}$ with respect to probe 8, while probe 17 and 18 are placed at $x = 90\,\mathrm{mm}$ and $x = 180\,\mathrm{mm}$. The right-handed coordinate system is completed by the z-axis, which is parallel to the beam axis pointing downstream. The support of the Hall probes is mounted on a special support system, which allows for a longitudinal movement in z-direction in steps of $\Delta z = 50\,\mathrm{mm}$. Furthermore individual positions on the x-axis were adjustable in steps of $\Delta x = 20\,\mathrm{mm}$. The alignment of the entire measurement apparatus with respect to the magnet and the beam axis is described in Refs. [5–7].

2.1 Procedure

Four data sets using different settings of the power converters have been obtained during the measurement campaign. For each data set the horizontal position x was varied in discrete steps. The z-axis of the coordinate system is supposed to be parallel to the beam axis of the H4 beamline (see Figure 4). At each x-position the Hall probe carrier was moved longitudinally starting from $z = -1750\,\mathrm{mm}$ up to $+1850\,\mathrm{mm}$ in steps of $\Delta z = 50\,\mathrm{mm}$[1]. The magnetic field distribution in vertical direction is obtained

[1] A few measurements were taken with longitudinal steps of $\Delta z = 300\,\mathrm{mm}$ to allow for a larger set of measurements in x-direction in the same measurement time.

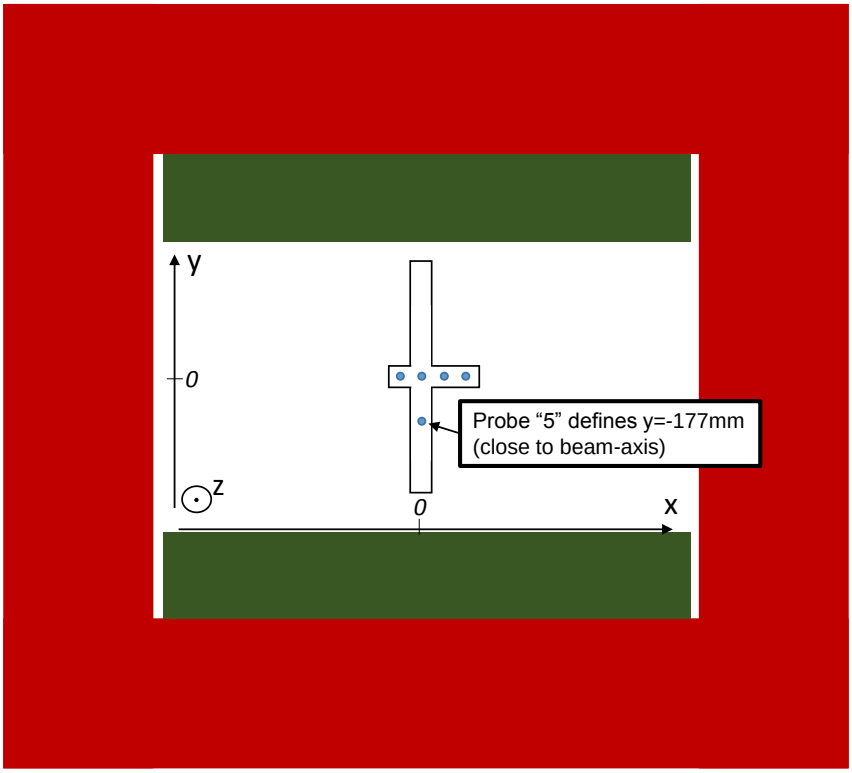

Fig. 4: Schematic drawing of the probe apparatus within the GOLIATH magnet.

by the arrangement of the first 15 Hall probes. Five consecutive field measurements were taken with each of the Hall probes at each (x, z)-point to obtain a three dimensional representation of the magnetic field. Table 1 summarizes an overview of the measurements taken at different currents and horizontal positions.

Table 1: Overview of the taken measurements at different power converter configurations (G=GOLIATH, D=DAVID)

I_{G} (A)	I_{D} (A)	x-position (cm)
3600	1750	-72, -60, -48, -36, -16, -12, -8, -4, 0, 4, 8, 12, 16, 36, 48, 60, 72, 84
2400	1166.7	-72, -60, -48, -36, -16, -12, -8, -4, 0, 4, 8, 12, 16, 36, 48, 60, 72, 84
1200	583.3	-16, -4, 0, 4, 84
3600	0	-8, -4, 0, 4, 8

2.2 Uncertainty Estimates

The measurement set at $I_{\mathrm{G}} = 3600\,\mathrm{A}$ and $I_{\mathrm{D}} = 1750\,\mathrm{A}$ is used to estimate the statistical uncertainty. For the five measurements at each (x, z)-point the sample mean $\bar{B}_y$ and corrected sample standard deviation $\sigma^*_{\bar{B}_y}$ is calculated for the B_y-component of the field for each of the first 15 hall probes according to:

$$\bar{B}_y = \frac{1}{5}\sum_{i=1}^{5} B_{y,i}\ , \tag{1}$$

$$\sigma^*_{\bar{B}_y} = \sqrt{\frac{1}{5-1}\sum_{i=1}^{5}\left(B_{y,i} - \bar{B}_y\right)^2}\ . \tag{2}$$

The ratio of both values is illustrated in Figure 5 summarizing all measurements of B_y taken at this power converters configuration. The fitted red line corresponds to a constant value of $\sigma_{B_y} = 18.5\,\mu\mathrm{T}$. Three groups of 15 points are observable with a larger ratio, which indicate a negligible instability of

the field during these measurements. The blue line illustrates the estimate of the systematic error of $\sigma_{B_y} = 0.2\,\mathrm{mT}$ [8]. Since the statistical errors are about an order of magnitude smaller than the measured field strengths, they are neglected for the rest of the analysis.

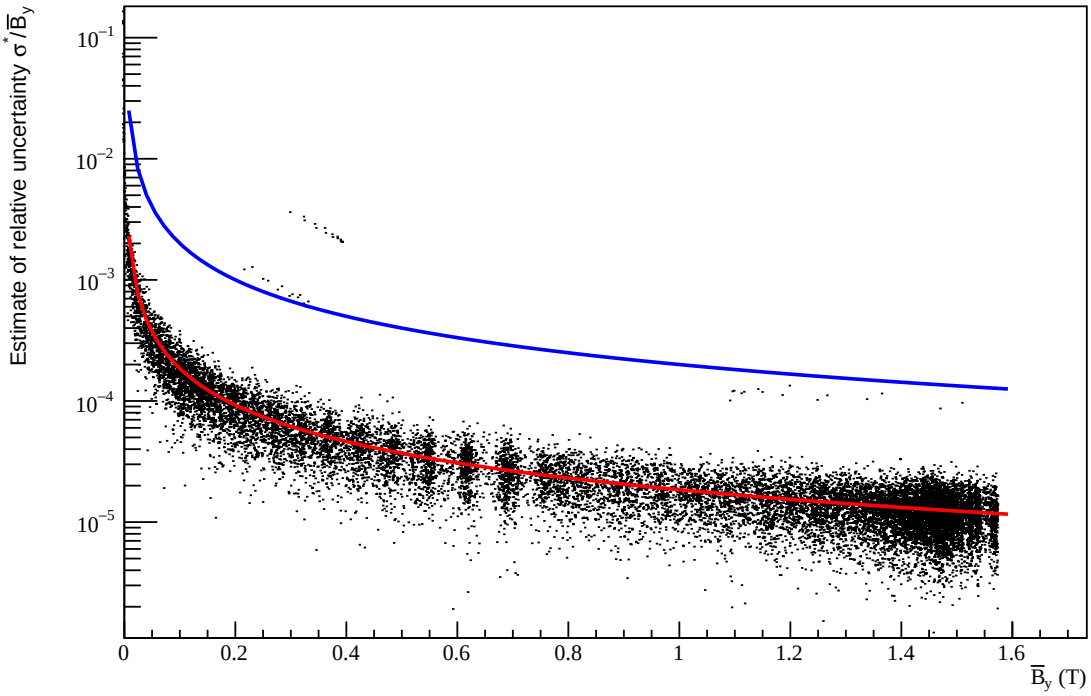

Fig. 5: Estimation of the statistical and systematical uncertainties. The red curve describes a fit to the calculated relative statistical uncertainties corresponding to a constant value of $\sigma_{B_y} = 18.5\,\mu\mathrm{T}$. The blue curve reflects the systematic error estimate of $\sigma_{B_y} = 0.2\,\mathrm{mT}$ [8].

2.3 Fieldmap Interpolation

An efficient interpolation method had to be chosen in order to obtain an equally-spaced full three-dimensional grid of the magnetic field based on the recorded data. Two different methods have been investigated for their efficiency. The first method is a linear interpolation of the neighboring points, while in the second method a spline interpolation as implemented in ROOT v.6.06/08 [9] is used. As an example, the measurements at $I_\mathrm{G} = 2400\,\mathrm{A}$ and $I_\mathrm{D} = 1166.7\,\mathrm{A}$ are discussed. Three measurements of the vertical magnetic field along the z-direction at $x = 0\,\mathrm{mm}$ but different vertical positions are chosen to illustrate the difference between the interpolation routines. Each of these measurements was taken with a longitudinal step size of $\Delta z = 50\,\mathrm{mm}$. Based on the data set, a new artificial data set with a coarse spacing of $\Delta z = 300\,\mathrm{mm}$ was created by taking only every sixth point. The interpolation routines are applied on these new data sets and compared to the original data. The results are shown in Figure 6 and Figure 7. While the colored lines in Figure 6a and Figure 7a display the measured data with finer spacing, the associated black lines correspond to the interpolated data. In addition, the difference between both curves normalized to the central magnetic field value is calculated and displayed in Figure 6b and Figure 7b. It can be seen that there is a good agreement between measurement and interpolation. In case of the linear interpolation, the differences between measured and interpolated points amounts to up to 6%, due to the steep field falloff. For the spline interpolation, the differences are reduced to up to 2%. Hence, the spline interpolation has been chosen for the entire data illustrated in the following sections.

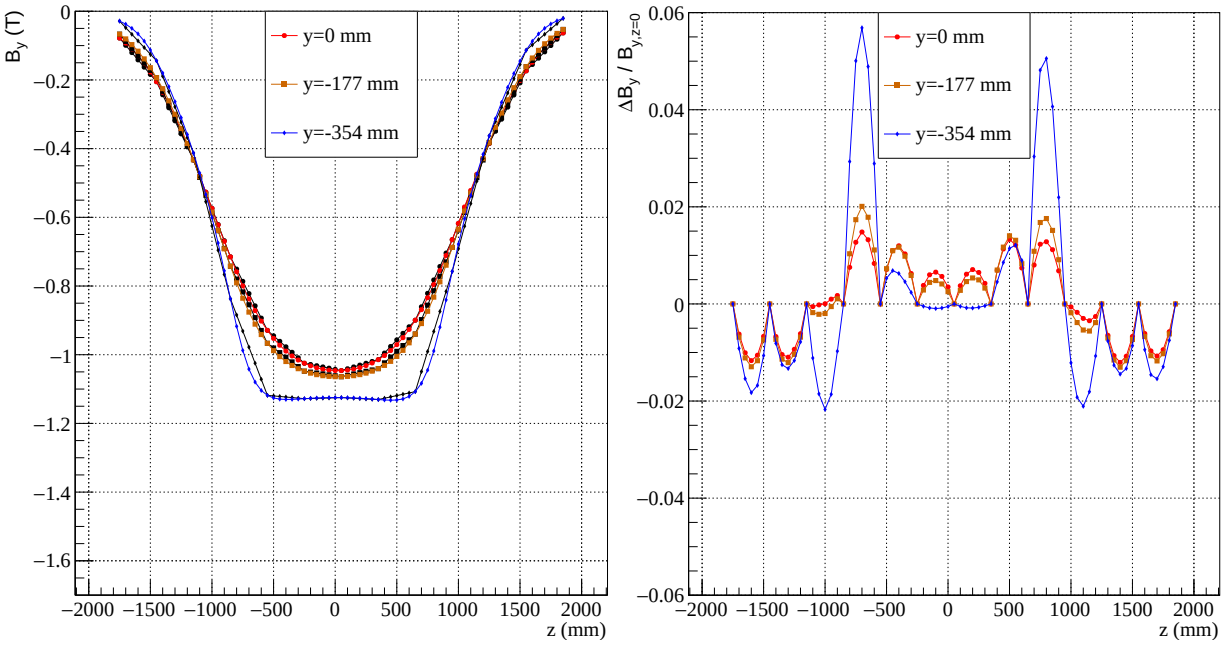

(a) (b)

Fig. 6: (a): Measurement of the vertical magnetic field at $I_{\mathrm{G}} = 2400\,\mathrm{A}$ and $I_{\mathrm{D}} = 1166.7\,\mathrm{A}$. The lines joining the points correspond to a linear interpolation assuming only every sixth point was taken as discussed in the text. (b): Difference of the real measurement and the linear interpolation normalized to the central field value.

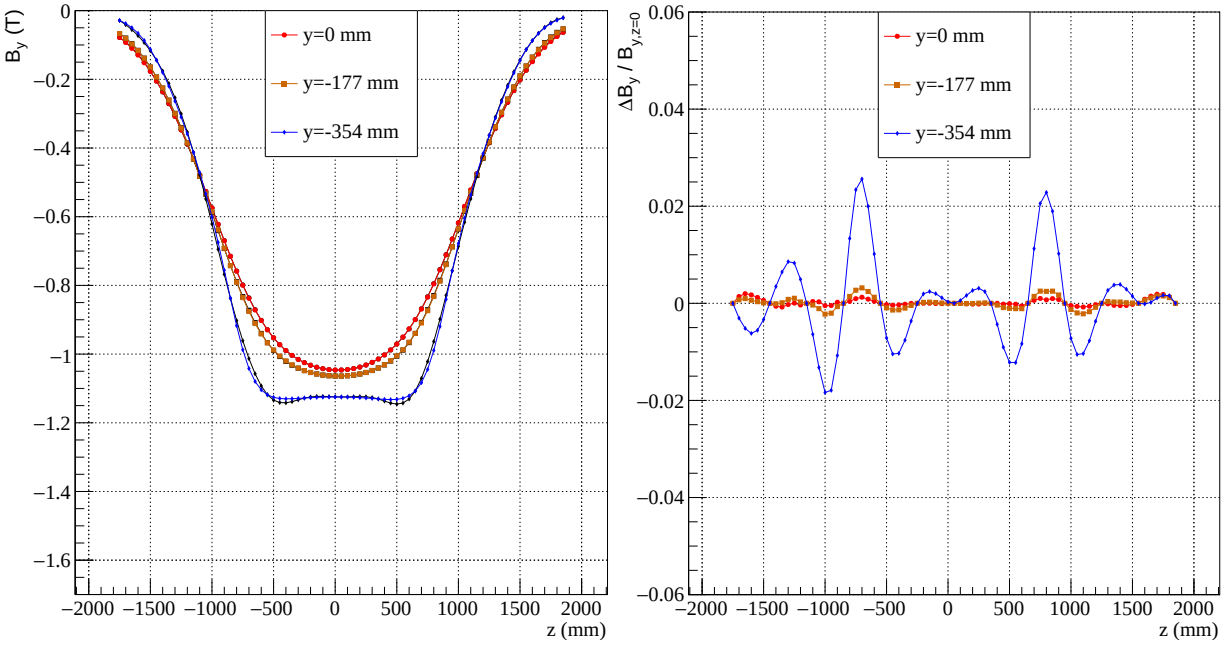

(a) (b)

Fig. 7: (a): Measurement of the vertical magnetic field at $I_{\mathrm{G}} = 2400\,\mathrm{A}$ and $I_{\mathrm{D}} = 1166.7\,\mathrm{A}$ The lines joining the points correspond to a spline interpolation assuming only every sixth point was taken as discussed in the text. (b): Difference of the real measurement and the linear interpolation normalized to the central field value.

3 Results for Nominal Configuration

This section summarizes the analysis of the field measurements obtained for an equal field produced in upper and lower coil using GOLIATH and DAVID power converters. First, the shape of the vertical magnetic field and its behavior for different scalings of the currents is explored. Additionally, hysteresis effects are quantified. In the subsequent step, the integrated field is calculated using an analytical description of the central vertical magnetic field. The obtained values are compared to an existing GOLIATH field measurement obtained in the 1980s [4]. Finally, the horizontal and longitudinal field components are discussed and compared to the existing field measurement.

3.1 Shape of the Vertical Magnetic Field

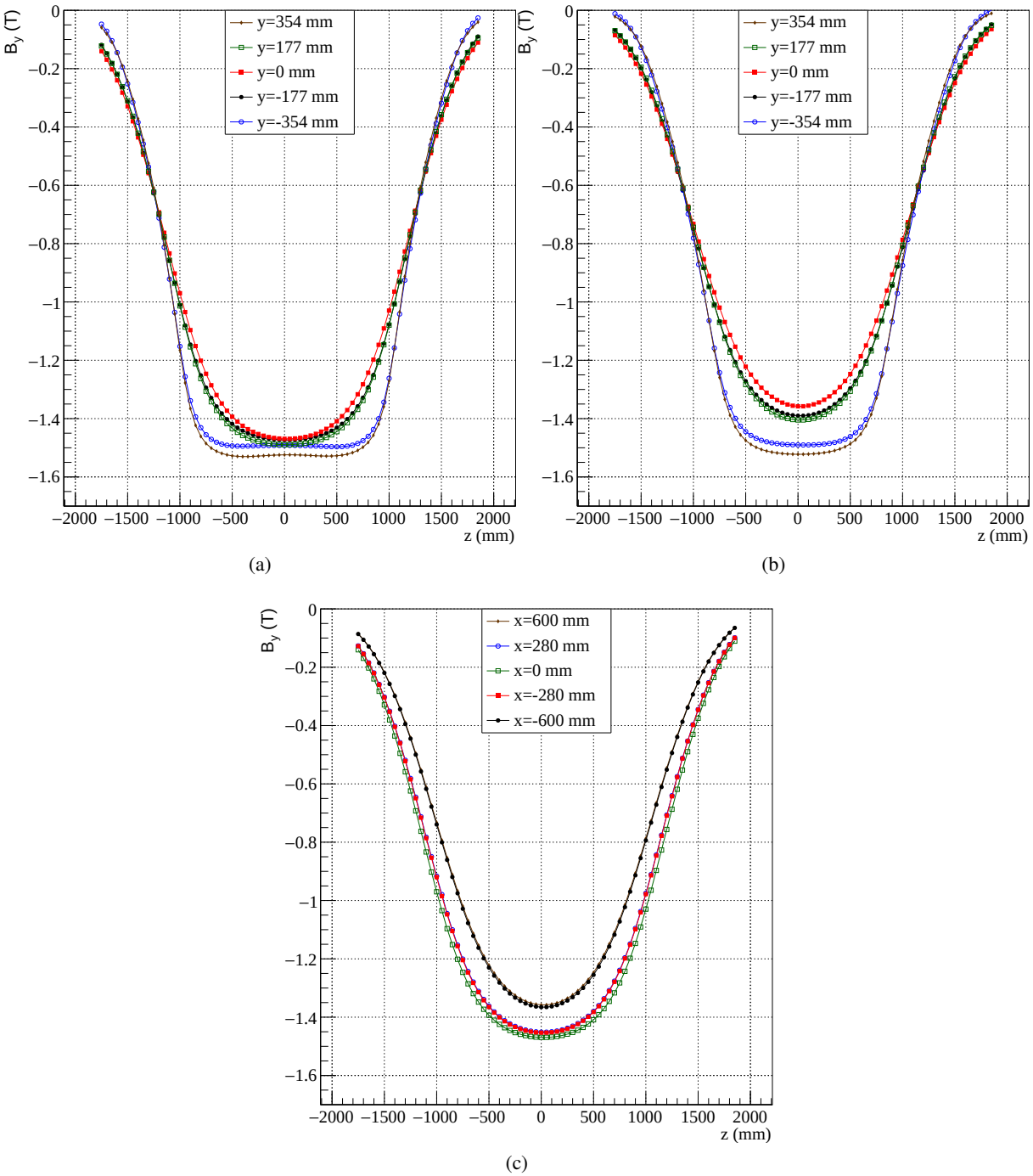

Fig. 8: Measurement of the vertical magnetic field at $I_{\mathrm{G}} = 3600\,\mathrm{A}$ and $I_{\mathrm{D}} = 1750\,\mathrm{A}$ for (a) $x = 0\,\mathrm{mm}$, (b) $x = 600\,\mathrm{mm}$, (c) $y = 0\,\mathrm{mm}$.

The shape of the vertical magnetic field along the z-direction is illustrated in Figure 8 for $x = 0\,\mathrm{mm}$, $x = 600\,\mathrm{mm}$ and $y = 0\,\mathrm{mm}$ and power converter currents of $I_\mathrm{G} = 3600\,\mathrm{A}$ and $I_\mathrm{D} = 1750\,\mathrm{A}$. Note that positive currents in the power converters lead to a negative vertical magnetic field. In the central region the field possesses a parabolic shape, while it becomes shaped trapezoidally for bigger vertical offsets y. At the same time the field strength in the central region also increases towards larger y. Considering the horizontal direction the magnetic field decreases for larger x-positions, but still preserves its parabolic shape.

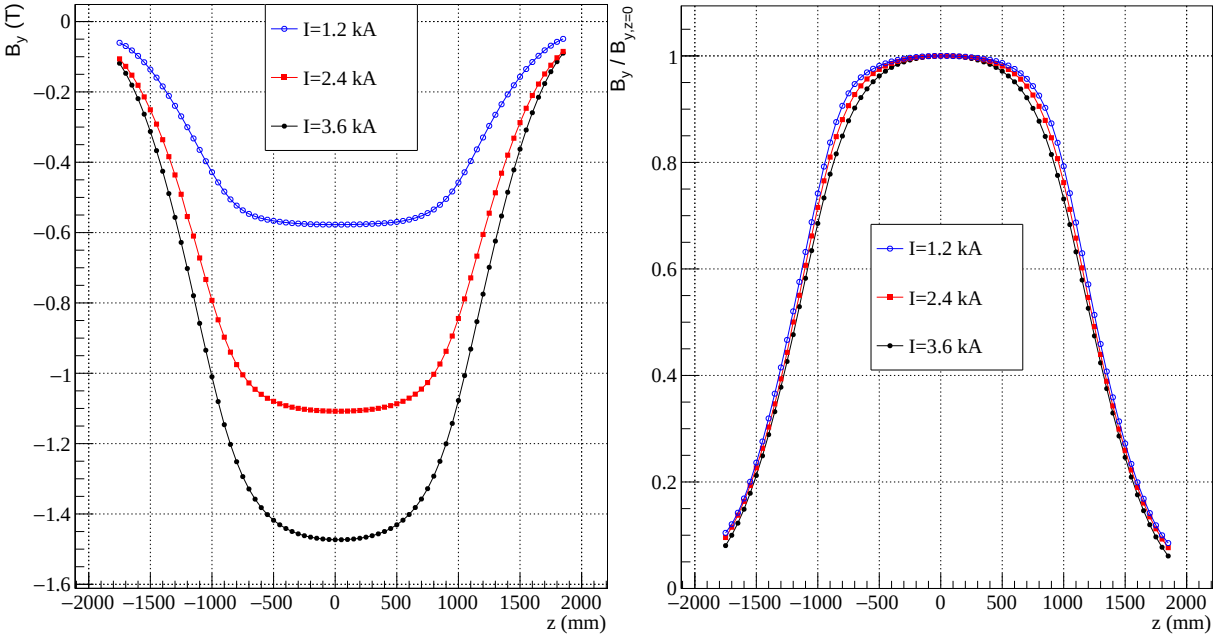

(a) (b)

Fig. 9: (a): Measurement of the vertical magnetic field at at $(x, y) = (0\,\mathrm{mm}, -177\,\mathrm{mm})$ for different currents $I_\mathrm{G}, I_\mathrm{D}$. The graphs are described by its current I_G, but the current I_D was changed accordingly. (b): Vertical magnetic field normalized to its central value to illustrate the differences of the shape for different currents.

Figure 9 shows the vertical magnetic field at $(x, y) = (0\,\mathrm{mm}, -177\,\mathrm{mm})$ for different currents $I_\mathrm{G}, I_\mathrm{D}$. For comparison, they have also been normalized to the value at $z = 0\,\mathrm{mm}$. This reveals a similar effect for smaller currents: the field shape transforms from parabolic to trapezoidal.

3.2 Impact of Hysteresis

The yokes of the GOLIATH magnet consist of iron and thus the magnetic field could be prone to hysteresis effects. To evaluate the magnitude of this effect, two measurements of the magnetic field based on a different ramp-up process of the magnetic field were performed. The final currents were set to $I_\mathrm{G} = 2400\,\mathrm{A}$ and $I_\mathrm{D} = 1166.7\,\mathrm{A}$. The first measurement was obtained by ramping the power converters first to $I_\mathrm{G} = 3600\,\mathrm{A}$ and $I_\mathrm{D} = 1750\,\mathrm{A}$ before applying the final currents. For the second measurement the power converters were initially turned off before the final currents were applied. Figure 10 shows the vertical magnetic field measurements for both scenarios at $x = 0\,\mathrm{mm}$ and three different vertical positions. Additionally, the differences normalized to the central magnetic field value are presented, being below $2\,‰$. Hence, the effect of hysteresis created in the scenario described is three orders of magnitude smaller than the central field values. This reveals the good reproducibility of the field strengths when using the same powering scheme and the hysteresis effects can be neglected in the rest of the analysis.

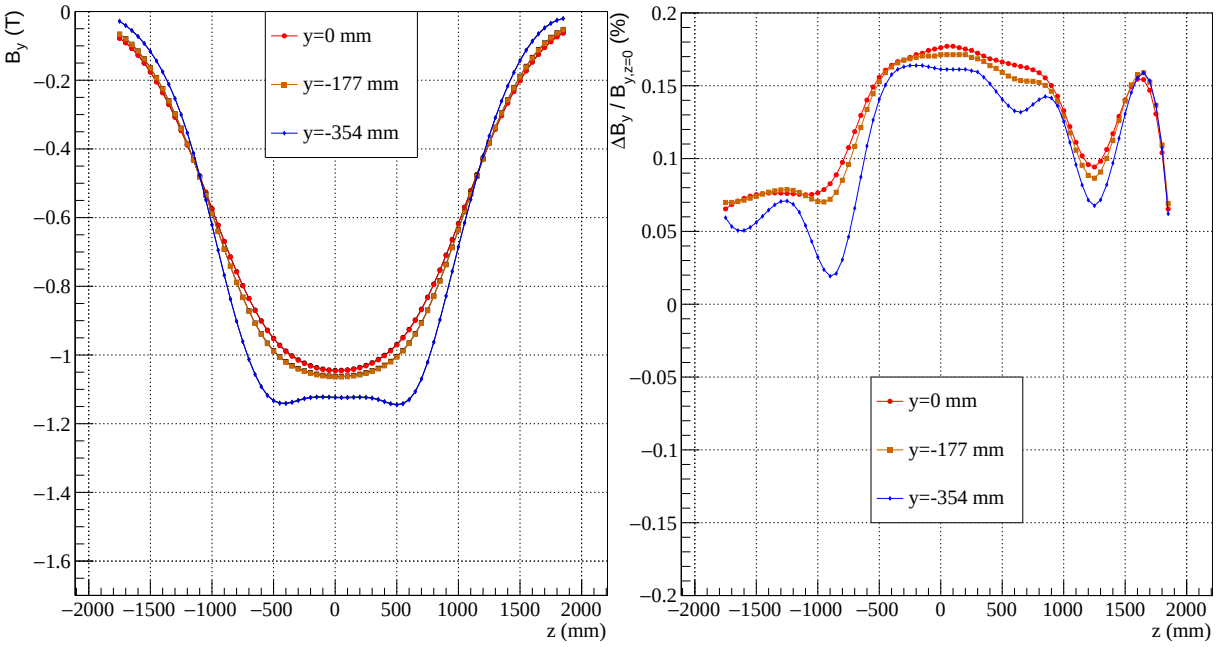

(a) (b)

Fig. 10: (a): Measurements of the vertical magnetic field at $I_\mathrm{G} = 2400\,\mathrm{A}$ and $I_\mathrm{D} = 1166.7\,\mathrm{A}$. To identify the contribution from hysteresis, measurements were taken either after ramping to $I_\mathrm{G} = 3600\,\mathrm{A}$ and $I_\mathrm{D} = 1750\,\mathrm{A}$ and returning to the final currents (colored points) or after turning off the power converters and returning to the target currents (black points, almost in agreement with the colored points). (b): Differences between both measurements normalized to the central magnetic field value.

3.3 Integrated Vertical Magnetic Field

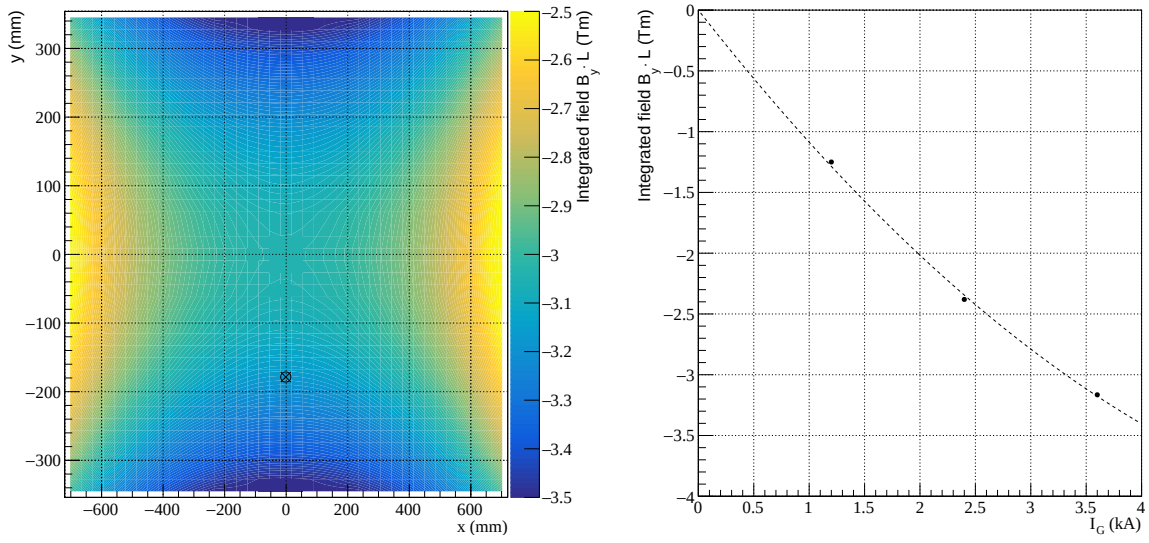

(a) (b)

Fig. 11: (a): Measured vertical magnetic field integrated from $z = -1750\,\mathrm{mm}$ to $z = 1850\,\mathrm{mm}$. The black marker indicates the beam entry point. (b): Integrated magnetic field curve as function of the current of the GOLIATH power converter obtained at $(x, y) = (0\,\mathrm{mm}, -177\,\mathrm{mm})$. The DAVID power converter was scaled accordingly to preserve an equal field produced in top and bottom coil.

The overall particle deflection can be estimated by the integrated vertical magnetic field. The integrated field has been calculated for the power converter settings $I_\mathrm{G} = 3600\,\mathrm{A}$ and $I_\mathrm{D} = 1750\,\mathrm{A}$ in the measurement range from $z = -1750\,\mathrm{mm}$ to $z = 1850\,\mathrm{mm}$ and for constant x and y. The variations

for different x and y are illustrated in Figure 11a. Based on the alignment measurements (described in Refs. [5–7]), the beam entry point is calculated to be at $(x, y) = (-1.4\,\mathrm{mm}, -178.6\,\mathrm{mm})$, with respect to the measurement coordinate system. This point is indicated by the black marker.

Figure 11b illustrates the variation of the integrated vertical magnetic field for the different power converter settings. A second order polynomial is used to empirically describe the field variation demanding a zero field value at zero current:

$$(B_y \cdot L)(I_\mathrm{G}) = p_1 \cdot I_\mathrm{G} + p_2 \cdot I_\mathrm{G}^2 \,, \tag{3}$$

$$p_1 = -1.166\,\mathrm{Tm/kA} \,, \tag{4}$$

$$p_2 = 0.079\,\mathrm{Tm/kA}^2 \,, \tag{5}$$

$$I_\mathrm{D} = \frac{35}{72} I_\mathrm{G} \,. \tag{6}$$

3.4 Comparison to prior Measurements

To validate the measurement and analysis of the vertical magnetic field, the recorded data is compared to an already existing data set from the 1980s [4]. In this measurement campaign the field values had been obtained in the range:

$$x \in \{-1120\,\mathrm{mm}, 1160\,\mathrm{mm}\} \,, \tag{7}$$

$$y \in \{-450\,\mathrm{mm}, 450\,\mathrm{mm}\} \,, \tag{8}$$

$$z \in \{-2400\,\mathrm{mm}, 2460\,\mathrm{mm}\} \,. \tag{9}$$

The vertical magnetic field is extracted along z for $x = 0\,\mathrm{mm}$ and for the central region $y = -177\,\mathrm{mm}$,$y = 0\,\mathrm{mm}$ and $y = 177\,\mathrm{mm}$ for both data sets. The field can be described analytically, also including the fringe field regions. For that purpose, the falloff in the fringe field regions is characterized by two Enge functions [10] similar to the implementation used in the COSY Infinity [11] framework:

$$\begin{aligned} B(z) &= B_0 \cdot F(z_a) \cdot F(z_b) \,, \\ F(\tilde{z}) &= \frac{1}{1 + \exp\left(a_1 + a_2 \cdot \tilde{z} + \cdots + a_6 \cdot \tilde{z}^5\right)} \,, \\ z_a &= \frac{z - z_0 - 1165\,\mathrm{mm}}{1060\,\mathrm{mm}} \,, \quad z_b = \frac{-z + z_0 - 1165\,\mathrm{mm}}{1060\,\mathrm{mm}} \,. \end{aligned} \tag{10}$$

For the above calculations, the gap opening between the yokes of $1060\,\mathrm{mm}$ and an effective field boundary of about $1165\,\mathrm{mm}$ is used.

The analytical formula has been fitted to old and new data set to obtain the free parameters. Results are illustrated in Figure 12. The left figures show the data points together with the fit results, the right figures show the difference normalized to the central field value, respectively. In all cases, these relative differences are well below 1% proving a good analytical description of the measured data. The old and new data set are not directly comparable, since the measurement coordinate systems posses a slight offset with respect to each other. In the old data set the origin is slightly below the magnetic center, while in the new data set it is slightly above.

The fit parameters of the six curves are summarized in Table 2 and Table 3 It can be seen, that the parameter values obtained are quite similar. Once again, this confirms a good reproducibility and long-term stability of the field. Especially the difference of the parameters a_1 and a_2 for the different vertical offsets y is comparable in both independent analyses. The other parameters a_i are more sensitive to larger distances from the effective field boundary (large z_a or z_b) and due to the extended measurement range in the older data set, these values are constraint stronger in this set. The longitudinal magnetic center with respect to the measurement coordinate system is estimated to be between $1\,\mathrm{mm}$ and $2\,\mathrm{mm}$ in the old measurement, while it is about $23\,\mathrm{mm}$ in the new measurement.

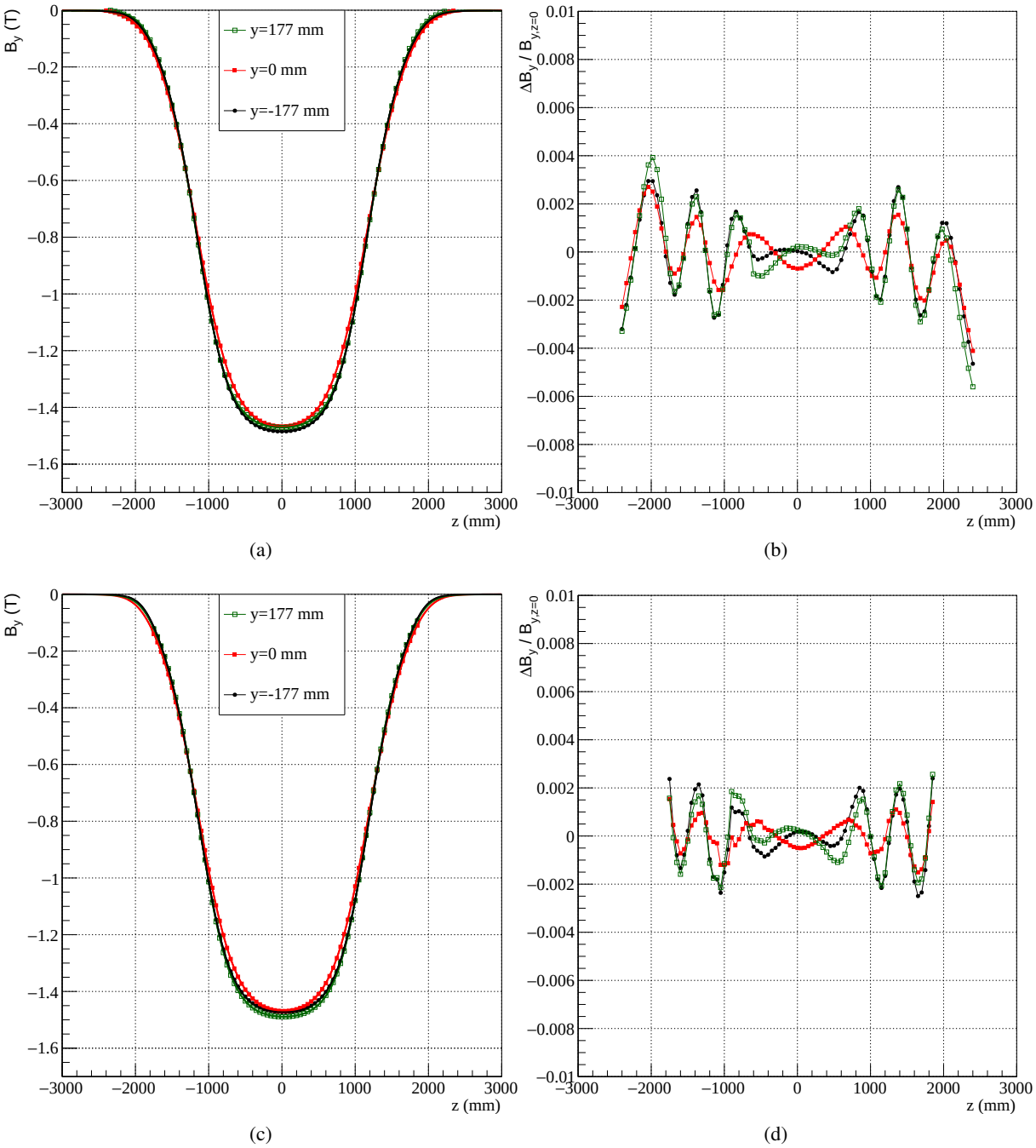

Fig. 12: Fits of analytical expressions according to Equation 10 to the measured vertical field of the (a) older data set and (c) new data set for $I_{\mathrm{G}} = 3600\,\mathrm{A}$, $I_{\mathrm{D}} = 1750\,\mathrm{A}$ and $x = 0\,\mathrm{mm}$. The differences between fit and measured data are shown in figures (b) for the older data set and (d) for the new data set.

Table 2: Resulting parameters of the fit of Equation 10 to the older data set at $I_G = 3600\,A$, $I_D = 1750\,A$ and $x = 0\,mm$.

	$y = -177\,cm$	$y = 0\,cm$	$y = 177\,cm$
B_0 (T)	-1.50867	-1.51752	-1.49273
z_0 (mm)	2.01171	1.54753	1.10607
a_1	-0.124782	-0.0905523	-0.163135
a_2	4.40763	3.91333	4.41989
a_3	-0.885277	-0.492688	-0.982521
a_4	-0.670369	-0.492261	-0.785681
a_5	0.319334	0.236191	0.286596
a_6	0.090873	0.065219	0.0869344

Table 3: Resulting parameters of the fit of Equation 10 to the new data set at $I_G = 3600\,A$, $I_D = 1750\,A$ and $x = 0\,mm$.

	$y = -177\,cm$	$y = 0\,cm$	$y = 177\,cm$
B_0 (T)	-1.4934	-1.51747	-1.51061
z_0 (mm)	23.5994	22.6964	22.5293
a_1	-0.160741	-0.0894863	-0.12814
a_2	4.43151	3.89419	4.44809
a_3	-0.983578	-0.5562188	-1.0414
a_4	-0.679163	-0.49327	-0.787396
a_5	0.332264	0.243234	0.289476
a_6	0.0893209	0.0643978	0.0855459

Due to the extended measurement range covering more of the fringe field region a slight increase of the calculated integrated field compared to the new data set is expected. Similar to Figure 11 for the new data set, the calculated values for the older data set are shown in Figure 13. A marker at the same position as for the new data set is used to estimate the entry point of the beam. Besides the direct measurements, also the analytical fits can be used to calculate the integrated magnetic field. The

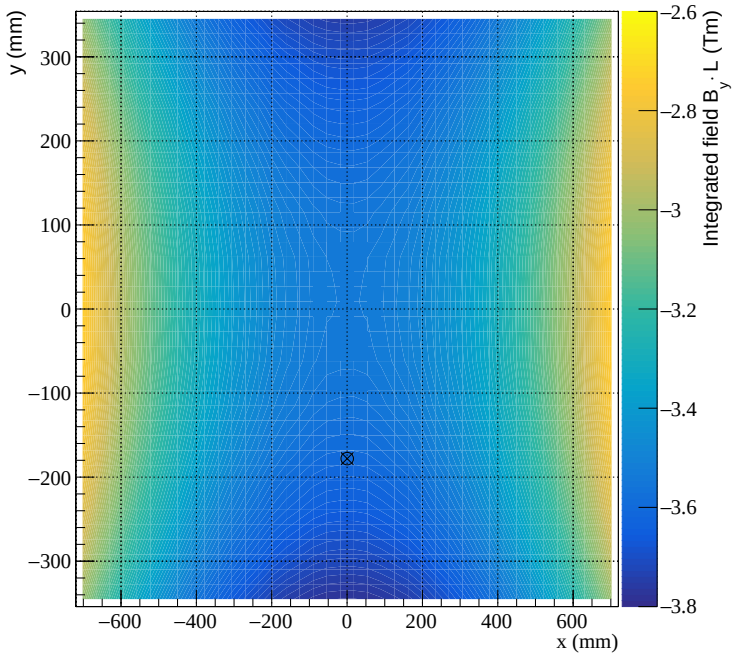

Fig. 13: Measured vertical magnetic field integrated from $z = -2400\,mm$ to $z = 2450\,mm$ for the older dataset from the 1980s. The black marker indicates the beam entry point.

Table 4: Integrated vertical magnetic fields for $I_{\mathrm{G}} = 3600\,\mathrm{A}$ and $I_{\mathrm{D}} = 1750\,\mathrm{A}$.

	$y = -177\,\mathrm{cm}$	$y = 0\,\mathrm{cm}$	z-range
Meas. [old] (Tm)	-3.585	-3.534	$-2.40\,\mathrm{m} \ldots 2.45\,\mathrm{m}$
Meas. [new] (Tm)	-3.165	-3.038	$-1.75\,\mathrm{m} \ldots 1.85\,\mathrm{m}$
Fit [old] (Tm)	-3.593	-3.536	$-5.00\,\mathrm{m} \ldots 5.00\,\mathrm{m}$
Fit [new] (Tm)	-3.571	-3.534	$-5.00\,\mathrm{m} \ldots 5.00\,\mathrm{m}$

integrated field strengths at $(x, y) = (0\,\mathrm{mm}, 0\,\mathrm{mm})$ and $(x, y) = (0\,\mathrm{mm}, -177\,\mathrm{mm})$ has been used for both measurements in their specific range and both analytical fits using a range from $-5\,\mathrm{m}$ to $5\,\mathrm{m}$ are summarized in Table 4. The older measurement and the two fits are in good agreement. In the new set of measurements the longitudinal range was not sufficient to cover the entire fringe field region, which can be also seen in Figure 12, but the missing part could be estimated to a good precision using the value from the analytical description.

The final step of the magnetic field analysis in the nominal configuration covers the shapes of the horizontal and longitudinal field components. They are subsequently compared between the older and the new data set for the power converter currents $I_{\mathrm{G}} = 3600\,\mathrm{A}$ and $I_{\mathrm{D}} = 1750\,\mathrm{A}$. Figure 14 illustrates the horizontal magnetic field component B_x for $x = 0\,\mathrm{mm}$ and different vertical positions. In case of a fully symmetric magnet, this component is expected to disappear. Indeed the measured B_x-values are below $10\,\mathrm{mT}$ for all vertical positions and thus very small compared to the vertical magnetic field.

Investigating the horizontal magnetic field component for $y = 0\,\mathrm{mm}$ and different radial positions allows drawing conclusions on the alignment of the coordinate system with respect to the magnetic field center. The measured data is illustrated in Figure 15. Also in this case a vanishing field is expected for a perfect alignment and a symmetric magnet. In the new data set the recorded field increases to positive values for an increasing x-coordinate. This hints for a small vertical offset of the coordinate system with respect to to the magnetic center in positive direction as mentioned earlier. Simultaneously the horizontal field vanishes for $x = 0\,\mathrm{mm}$, which shows a perfect radial alignment of the coordinate system with the magnetic center of the magnet. In the older data set the field decreases to positive values for an increasing x-coordinate, from which a negative vertical offset of the coordinate system with respect to to the magnetic center can be deduced. Furthermore, a systematic fluctuation of the field values at same z-coordinate is observed, while in the new data set the measured values still vary smoothly along z.

The longitudinal field variation along z shown in Figure 16 for different y-positions reflects the typical behaviour of this field component in the fringe fields of a dipole magnet. In the region where the beam passes ($y \approx -177\,\mathrm{mm}$) the field can take up values of more then $0.2\,\mathrm{T}$. According to Ampere's circuital law

$$\frac{\partial B_y}{\partial z} - \frac{\partial B_z}{\partial y} = 0\,, \tag{11}$$

the largest variation of B_z with respect to the vertical position is expected to be at the maximum slope of B_y along z. This is confirmed by both data sets, which also show a very good agreement of the shapes measured.

For different x-positions the longitudinal field component is depicted in Figure 17. For a perfect alignment a vanishing field is expected for all horizontal positions. Indeed, small field values below $20\,\mathrm{mT}$ are observed in the new measurement data. Additionally, the older data set shows larger fluctuations at this scale, which can be observed especially in the region between $z = 0\,\mathrm{mm}$ and $z = 1000\,\mathrm{mm}$.

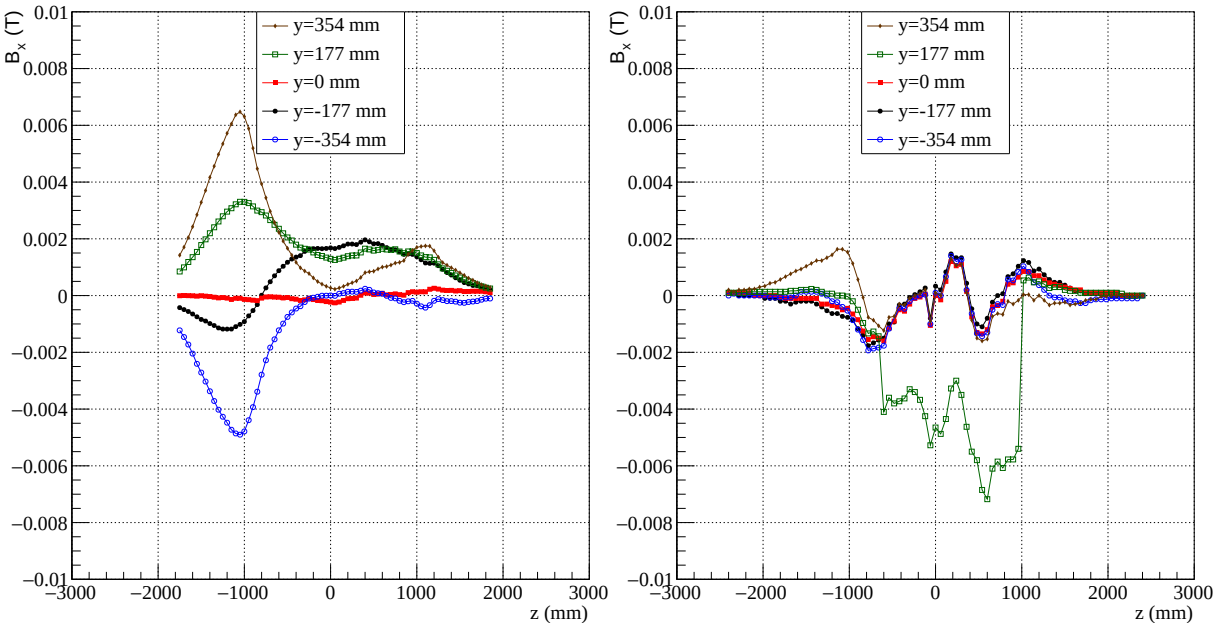

(a) (b)

Fig. 14: Measurement of the horizontal magnetic field at $I_{\mathrm{G}} = 3600\,\mathrm{A}$ and $I_{\mathrm{D}} = 1750\,\mathrm{A}$ at $x = 0\,\mathrm{mm}$ for (a) the new data set and (b) the older data set.

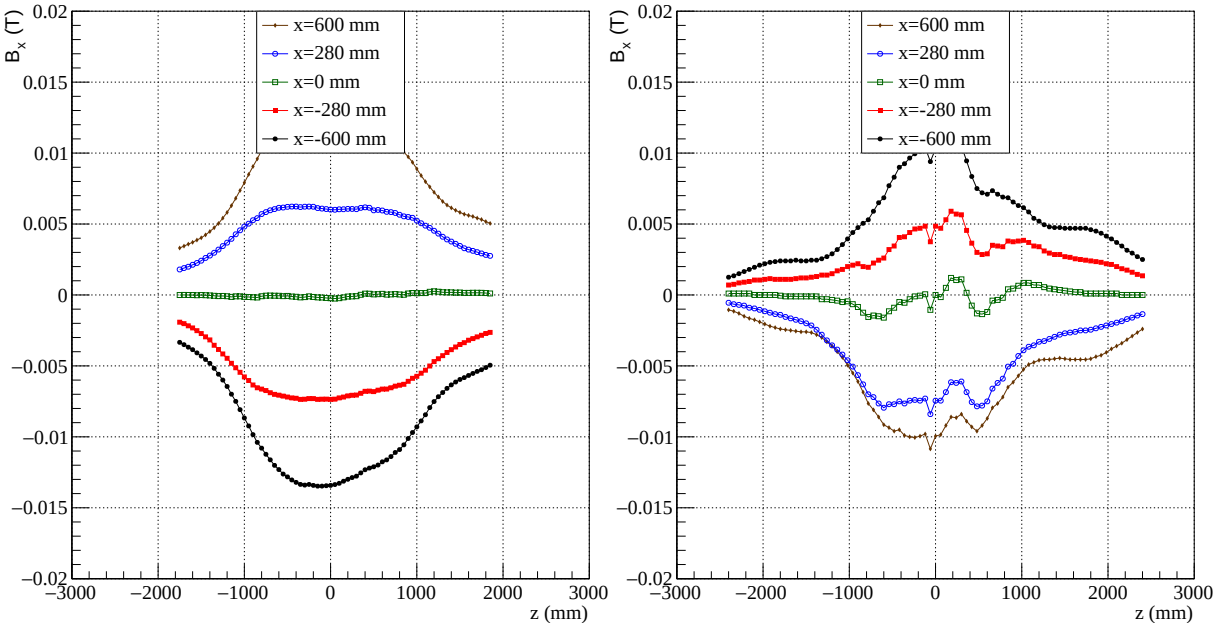

(a) (b)

Fig. 15: Measurement of the horizontal magnetic field at $I_{\mathrm{G}} = 3600\,\mathrm{A}$ and $I_{\mathrm{D}} = 1750\,\mathrm{A}$ at $y = 0\,\mathrm{mm}$ for (a) the new data set and (b) the older data set.

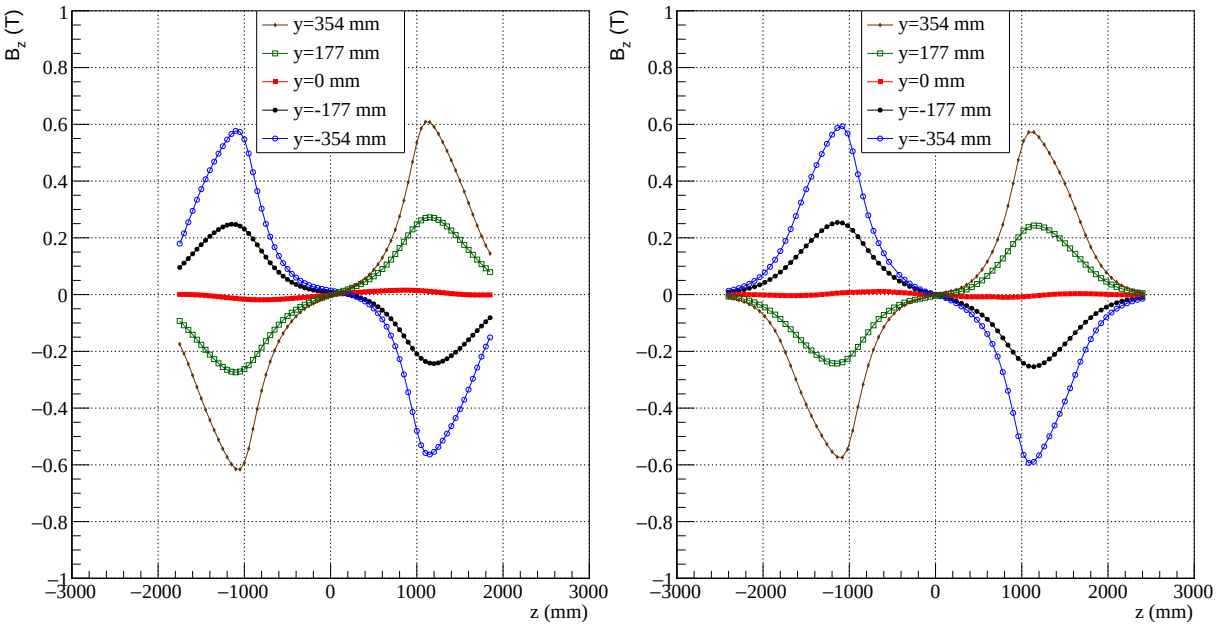

(a) (b)

Fig. 16: Measurement of the longitudinal magnetic field at $I_{\mathrm{G}} = 3600\,\mathrm{A}$ and $I_{\mathrm{D}} = 1750\,\mathrm{A}$ at $x = 0\,\mathrm{mm}$ for (a) the new data set and (b) the older data set.

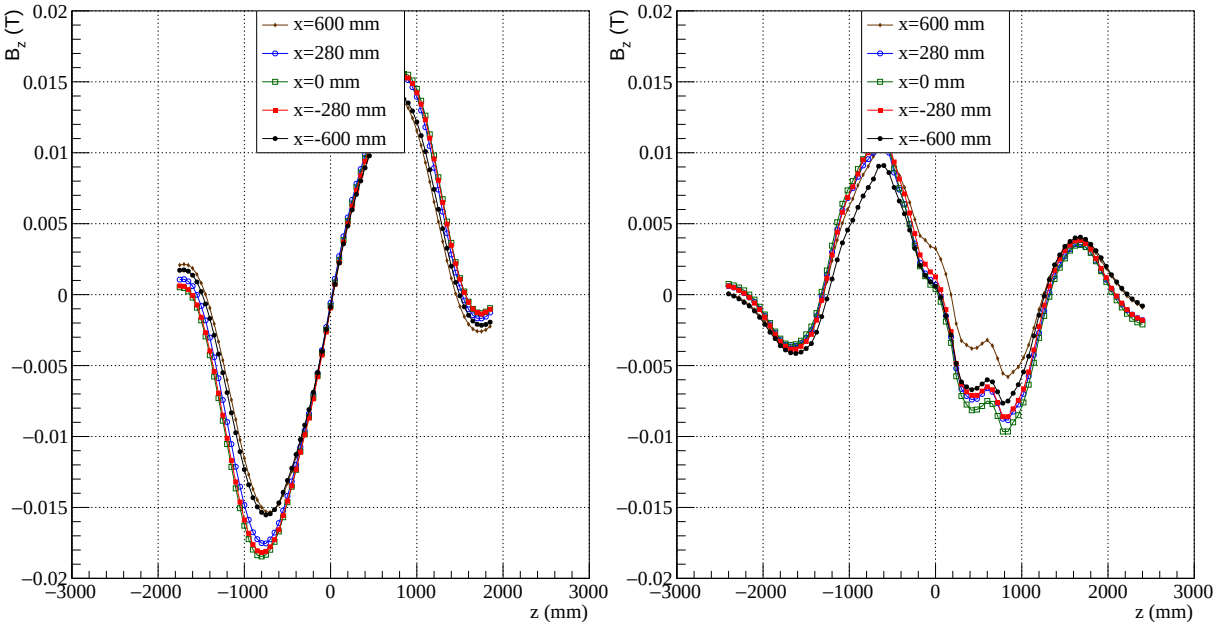

(a) (b)

Fig. 17: Measurement of the longitudinal magnetic field at $I_{\mathrm{G}} = 3600\,\mathrm{A}$ and $I_{\mathrm{D}} = 1750\,\mathrm{A}$ at $y = 0\,\mathrm{mm}$ for (a) the new data set and (b) the older data set.

4 Results for GOLIATH Power Converter only

This section describes the magnetic field measurements obtained while only the GOLIATH power converter was active. This configuration leads to a different magnetic field magnitude generated by the upper and lower coil. Thus, some distortions of the magnetic field shape and a significant change of the integrated field are expected. As already shown in Table 1, the horizontal extent of the recorded data set for this setup is limited to the central region. Hence, only variations with respect to the vertical positions will be discussed in the following. Additionally, also the alignment of the measurement apparatus was slightly different compared to the recorded data described before.

4.1 Magnetic Field Shape

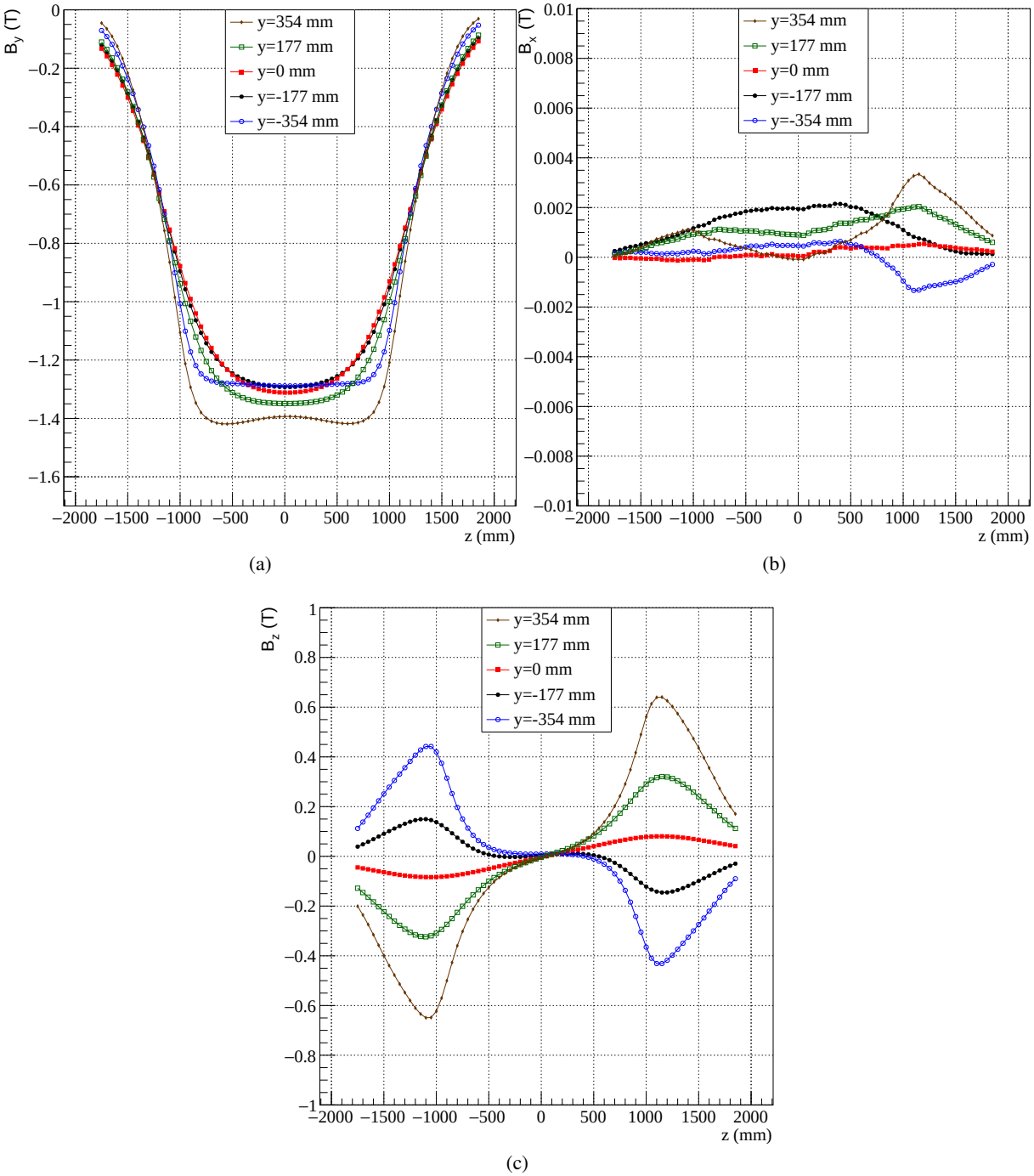

Fig. 18: Measurement of the (a) vertical, (b) horizontal and (c) vertical magnetic field at $I_{\mathrm{G}} = 3600\,\mathrm{A}$ and $I_{\mathrm{D}} = 0\,\mathrm{A}$ at $x = 0\,\mathrm{mm}$.

Figure 18 illustrates the variation of the three field components B_x, B_y and B_z along z for $I_\mathrm{G} = 3600\,\mathrm{A}$ and $I_\mathrm{D} = 0\,\mathrm{A}$. The vertical magnetic field strength is decreased as expected. The minimum value at the center is shifted to negative y due to the decreased magnetic field generated by the lower coil. The shape of the vertical magnetic field at $y = 354\,\mathrm{mm}$ now significantly differs from $y = -354\,\mathrm{mm}$. This imbalance is also clearly observable in the longitudinal field component. The maximum values of B_z for $y = 354\,\mathrm{mm}$ is increased compared to $y = -354\,\mathrm{mm}$, which is a consequence of the larger field generated by the upper coil.

Analogue to the previous section, the vertical magnetic field and its fringe field can be described by Enge functions using the parameters in Table 5.

Table 5: Resulting parameters of the fit of Equation 10 to the new data set at $I_\mathrm{G} = 3600\,\mathrm{A}$, $I_\mathrm{D} = 0\,\mathrm{A}$ and $x = 0\,\mathrm{mm}$.

	$y = -177\,\mathrm{cm}$	$y = 0\,\mathrm{cm}$	$y = 177\,\mathrm{cm}$
B_0 (T)	-1.3051	-1.34559	-1.36238
z_0 (mm)	22.3217	22.3166	22.7157
a_1	-0.174808	-0.113286	-0.163936
a_2	4.50221	4.01302	4.72307
a_3	-1.11482	-0.657048	-1.23902
a_4	-0.679098	-0.503267	-0.8197
a_5	0.339725	0.249432	0.303976
a_6	0.0876368	0.0628888	0.0816912

4.2 Integrated Vertical Magnetic Field

The integrated vertical magnetic field for this power converter configuration has been calculated. This is depicted in Figure 19. Note that the horizontal range only covers $-80\,\mathrm{mm}$ to $80\,\mathrm{mm}$ for this data set. The minimum of the integrated field is shifted to negative values due to the different powering of the

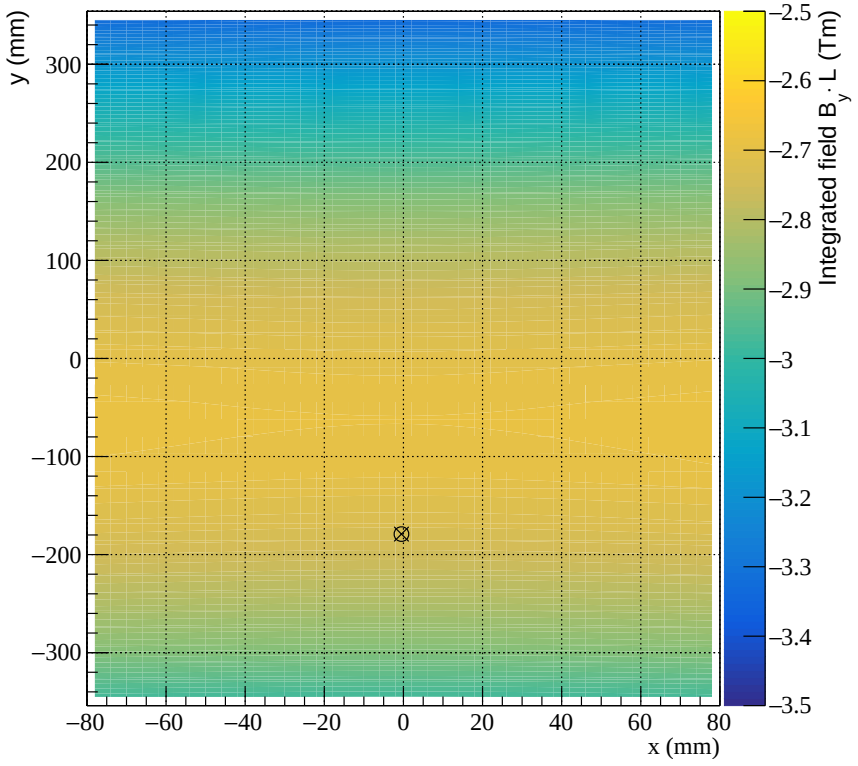

Fig. 19: Measured vertical magnetic field integrated from $z = -1750\,\mathrm{mm}$ to $z = 1850\,\mathrm{mm}$ for $I_\mathrm{G} = 3600\,\mathrm{A}$ and $I_\mathrm{D} = 0\,\mathrm{A}$. The black marker indicates the beam entry point.

Table 6: Integrated vertical magnetic fields for $I_{\mathrm{G}} = 3600\,\mathrm{A}$ and $I_{\mathrm{D}} = 0\,\mathrm{A}$.

	$y = -177\,\mathrm{cm}$	$y = 0\,\mathrm{cm}$	z-range
Meas. (Tm)	-2.734	-2.707	$-1.75\,\mathrm{m} \ldots 1.85\,\mathrm{m}$
Fit (Tm)	-3.161	-3.183	$-5.00\,\mathrm{m} \ldots 5.00\,\mathrm{m}$

coils as expected. The black marker is located at $(x, y) = (0.3\,\mathrm{mm}, -178\,\mathrm{mm})$ and corresponds to the estimated beam entry point taken from Refs. [5–7].

Similar to the previous section the measured integrated vertical magnetic field in the longitudinal range from $-1750\,\mathrm{mm}$ to $1850\,\mathrm{mm}$ has been calculated. Additionally also the integrated field resulting from the fit for $-5\,\mathrm{m}$ to $5\,\mathrm{m}$ has been obtained. The values are presented in Table 6.

5 Conclusion

During the measurement campaign of the magnetic field of the GOLIATH magnet conducted in 2017, a very good precision of all three field components could be obtained. Several data sets using different configurations of the power converters have been recorded. The statistical uncertainty was estimated to be smaller than $20\,\mu\mathrm{T}$, which is an order of magnitude smaller than the estimated systematic uncertainty. The vertical magnetic field could be described by analytical expressions, which were fitted to the measured data. A similar procedure has been applied to an older magnetic field measurement conducted in the 1980s. Overall a good agreement between both measurement campaigns was observed. The fits also enabled the calculation of the integrated vertical magnetic field close to the beam axis of the H4 beamline.

6 Acknowledgments

The authors would like to thank the physicists E. Oliveri and Y. Tsipolitis from RD51 collaboration for their support and for allowing us to take measurements during their beam time. Many gratitudes go to F. Antinori of NA57 experiment for providing the old field map and Y. Gaillard from the TE-EPC group for his support with the power converters.

7 References

[1] TE-EPC-HPC. http://te-dep-epc-hpc-section.web.cern.ch/te-dep-epc-hpc-section/spectrometers/Goliath/general.stm. *Webpage*, 12.12.2017.

[2] Y. Gaillard. Magnet specification 1969 - Note. *EDMS 1326984*, 1969.

[3] Y. Gaillard. Goliath archi - Schematics. *EDMS 1326980*, 2013.

[4] F. Antinori. Priv. Communication. *CERN*, 2017.

[5] D. Mergelkuhl. H4 TEST - GOLIATH MAGNET Measurement of B-field Machine Measurement Week 33 of 2017. *EDMS 1836813*, 2017.

[6] D. Mergelkuhl. H4 TEST - GOLIATH MAGNET Adjustment of B-field Machine Measurement Week 27 of 2017. *EDMS 1825777*, 2017.

[7] D. Mergelkuhl. H4 TEST - GOLIATH MAGNET - ADJUSTMENT OF B-FIELD MACHINE - Measurement of August 02nd, 2017. *EDMS 1834065*, 2017.

[8] F. Bergsma and H. Boterenbrood. A modular 3D magnetic-field sensor system with CANopen interface. *Proceedings of the 19th International Magnetic Measurement Workshop, NSRR, Hsinchu, Taiwan*, 2015.

[9] R. Brun and F. Rademakers. ROOT - An Object Oriented Data Analysis Framework. *Nucl. Inst. & Meth. in Phys. Res. A*, 389:81–86, 1997.

[10] M. Berz and K. Makino. Optics and nonlinear effects in repetitive systems. *Nucl. Inst. & Meth. in Phys. Res. A: Accelerators, Spectrometers, Detectors and Associated Equipment*, 645(1):175–181, 2011.

[11] M. Berz and K. Makino. COSY INFINITY 10.0 Beam Physics Manual. 2017.